Effect of Melting at Different Temperatures on the Structure and Mechanical Properties of Solder Alloy (Sn -Ag -In).

A.H. Al-Hammadi[(1)] F.A.Ghailan[(2)], F.A.H. Abu Hulaiqah[(1)]*
[(1)]*Physics Department , Faculty of Science , Sana'a University yemen.*
[(2)]*Physics Department Faculty of Education, Humanity of Applied Science Khawlan*
***Correspondent Author**: aregakrm12345@gmail.com (F.A.H. Abu Hulaiqah)*
DOI: https://doi.org/10.56807/buj.v3i3.226

Abstract

The aim of the present work is to prepare some samples of the alloy solders (Sn-2Ag-18In) at different temperatures(923,873,823,773 and 723k) to investigate some of their structure and different Mechanical properties as function of load and temperature ,The X-ray diffraction analysis of the samples ensures the formation of single phase hexagonal ,The average particle size estimated is(23.016 – 35.664)nm. Values of stress exponents (n) were found to be in the range of 0.575 to 3.822 for all alloys. Values of activation energy (Q) of alloys were found to be in the range of 0.287 to 1.899 ev .The average activation energy for the sample at different temperature's prepared , creep resistance and electrical conductivity of samples is calculated at room temperature (289k), its values found to be in the range of(900.6 - 10113.7)(Ω.cm)$^{-1}$.

*Keywords: Sn-Ag-In alloy solders ; Nano cr*ystal ; Mechanical properties.

ملخص

تأثير درجة حرارة الصهر على الخواص التركيبية ومقاومة الزحف والموصلية الكهربائية لسبيكة (القصدير -2 فضه-18انديوم) . قيست الخواص التركيبية ومقاومة الزحف والموصلية الكهربائية لسبائك (القصدير – 2 فضة -18 انديوم) باستخدام جهاز حيود الاشعة السينية وجهاز اختبار الزحف الميكانيكي ودائرة التيار المستمر , على التوالي . تم تحضير العينة بنقاوة عالية (99.99%) باستخدام تقنية الصهر في انابيب بيركس عند درجات حرارة مختلفة (923,873,823,773الى 723 كلفن). وقد اظهرت تحاليل جهاز حيود الاشعة السينية للسبيكة الثلاثية (قصدير - 2 فضة -18 انديوم)انها تتكون من طور احادي (طور سداسي) . متوسط الحجم الحبيبي لهذه العينات يتراوح بين (35.664 – 23.016) نانومتر بينما كثافة الانخلاعات تتزايد مع زيادة إضافة الفضة . وخصائص الزحف درست عند درجات حرارة مختلفة298 , 323, 353 كلفن) تحت تأثير ثلاثة احمال (6.2 , 8.7 , 12.5 ميجا باسكال). تم الحصول على قيم أس الاجهاد في نطاق ا (0.575الى 3.822) لجميع السبائك . تم الحصول على متوسط قيم طاقة التنشيط للسبائك في حدود 0.287 الى 1.899 الكترون فولت . وزحف المقاومة و الموصلية الكهربائية قيست عند درجة حرارة الغرفة(298 كلفن) قيمها تتراوح بين(900.6 الى10113.7)(اوم-سنتيمتر)$^{-1}$.

1.Introduction:

The toxic nature of lead has prompted the electronic packaging industry to seek environment alloy friendly Pb-free alloys as replacement to Pb-Sn solder alloy. Sn-Ag solders alloys have been considered as one of the most attractive lead free system that can replace toxic Sn-Pb solders without increasing the soldering temperature (Ahmed et al., 2010). Alloys solders (Sn–Pb) have been widely used in the field of electronic packaging because of its excellent characteristics, such as low melting point (183 °C), strong mechanical properties, low cost and low price (Peng et al., 2019, Zhang and Tu, 2014). Sn-Pb alloy welders, however are toxic. With the growing recognition of environmental protection and the issuance of the 'lead restriction order' by several countries, the use of Pb has been significantly reduced (Vuong et al., 2018, Zhu et al., 2019, Peng et al., 2019) . Lead-free solder alloys are typically Sn-based alloys due to the high corrosion resistance and good solder ability of tin (Sn) (S. Farina et al., 2014) . The Sn–Ag binary eutectic solder is one possible lead-free solder replacement for Sn–Pb. This alloy system is quite important because it is generally recognized as the first choice for lead-free solders, (M.M. EL-Bahay et al., 2004). It is well characterize the eutectic composition and temperature as Sn–3.5 wt.% Ag and 494 K, respectively. It possesses good ductility and better creep and thermal resistance than Sn–Pb solders. Although Sn–Ag eutectic solder melts at 494K compared to 458K of Sn–Pb eutectic solder, this may be acceptable for high temperature applications (D.R. Flanders et al.,1997). The tin–silver eutectic alloy has already been used in electronics soldering to a limited extent (Report Lead-Free Solders NASA Part., 1996). In addition, it is used for soldering of stainless steel for food processing applications. The Sn–In and Sn–Ag investigated solder alloys are already in practical use, but only in exactly determined conditions. Considering these, it could be expected that Ag–In–Sn ternary system might be one among the proper substitutes for common solders (A. Milosavlevic, et al.,2008). Although the Sn-Ag and Sn-Ag-Cu solders are the most widely studied solder systems because of their high strength, creep resistance, and excellent machinability. However, due to their high cost, they cannot be applied to large-scale production and processing (D.R. Frear .,2001) Previous investigation have shown that adding indium can decrease the melting point of the Sn-Ag and enhance the wettability between Sn-Ag-In solder alloy,(McAllister. W.D .2007) . This study investigates the effect of prepared temperatures on the microstructural and mechanical properties of the eutectic Sn-Ag-In solder alloy.

2. Experimental procedures

High purity metals Sn ,Ag ,and In were mixed together in molar ratio prepare mixed solder with the composition 80Sn-2Ag-18In to investigate some of their structure and some of their different mechanical properties. Alloys were prepared at different temperatures (923k ,873k, 823k,773k , and 723k) . The purity of Sn, Ag and In elements are about 99.99%. Every sample was put in electric furnace at (T=923k, 873k, 823k,773k , and 723k , about 2 hrs.) with shaking to achieve homogenization. To obtain samples fully precipitated phases, samples were left inside the furnace to solidify slowly to room temperature. The samples were polished using grades of silicon paper and then washed in a solution of (CH3COCH3), (Sh. Alsowidy., et al 2021). After that, the samples were drawn into two groups by using the rolling mechanism technique;. The first group was as wires of a diameter (D= 1 mm) and a length (L= 70 mm) for the creep properties testing. The second group was as small sheets for structural investigations (XRD). The samples were polished using grades of silicon paper and then washed in a solution of (CH3COCH3)(Sh.Alsowidy.,etal2021) . In order to remove residual stress and defects . X-ray Shimadzu DX-720 model with CuKα radiation with (λ=1.54056 Å) was used for XRD analysis. The XRD curves of the samples were constructed in the 2θ range of 5–75°. The operating source was under an accelerating voltage of 40 kV and a tube current 2 mA, with a constant scanning rate of 0.02/1sec. The tensile creep tests were implemented on all samples at different temperatures (298, 323, and 353K) under constant loads (6.2 , 8.7 and 12.5) MPa using a computerized vertical tensile technique. Electrical and conductivity are measured using a simple circuit (DC) of Ohm's law at room temperature

3. Results and discussion

The findings of this study are classified to structural, Mechanical and electrical properties of Sn-2Ag -18In alloys in concentrations as follows:

3.1. Structural analysis : The x-ray diffraction patterns for Sn-2Ag-18In at different temperature (T= 923k,873k,823k,773k , and 723k) were obtained at room temperature, using Cu-K_α at different temperature . The values of 2Ɵ-Bragg's angle , d-spacing for the recorded peaks and the corresponding relative intensities I/I_o (where I_o is the maximum intensity peak) for each pattern , and those obtained from JCPDS for 80Sn -20In are tabulated in the table (1). The prepared samples are tabulated in the tables (2,3,4,5,and 6). Accordance with values in JCOPDS in table (1) , it could be concluded that all prepared alloys were found to have single phase hexagonal structure . The x-ray diffraction patterns for the sample with prepared temperature 773k , it is found that ,the measured values of 2Ɵ-Bragg's angle shifted to the lower angle by 3.5^{o} . The density decrease of this sample , intermetallic particles with in the matrix is due to grain – boundary segregation or dissolution of the Sn Ag intermetallic . According to investigated materials structural, figure 1 (a, b , c ,d , and e) showed) respectively. The x-ray diffraction

(XRD) curves for (Sn–2Ag–18 In) solder at different prepared temperatures (923k,873k,823k,773k , and 723k) . The obtained diffraction patterns have been compared with standard powder diffraction data (pdf) using search / match process of measured data with appropriate reference file using the phase with **(**JCPDS-ICDD) Reference card no PDF#48-1547 . Figure (1a) showed the XRD results of80Sn-2Ag-18In alloy, which show: (i) large peaks intensity of primitive hexagonal , (ii) With single phase . The structure of Alloy , Phases Fig. 1(a ,b ,c ,d ,and e) . The phases respectively are marked in Figure 1(a, b ,c ,d and e). The particle sizes and dislocation density were studied as function of temperature as showed in Fig. (2). The particle size for the 80Sn–2Ag–18In alloys were calculated according to Scherer Formula (Williamson and Hall, 1953) : $D = \frac{0.9\,\lambda}{B\,\cos\theta}$ ---- (1),where: β is the broadening of diffraction line measured at half its maximum intensity (radians), D is the diameter of crystal particle, Θ is the Bragg's angle and λ is the wavelength of x-ray.

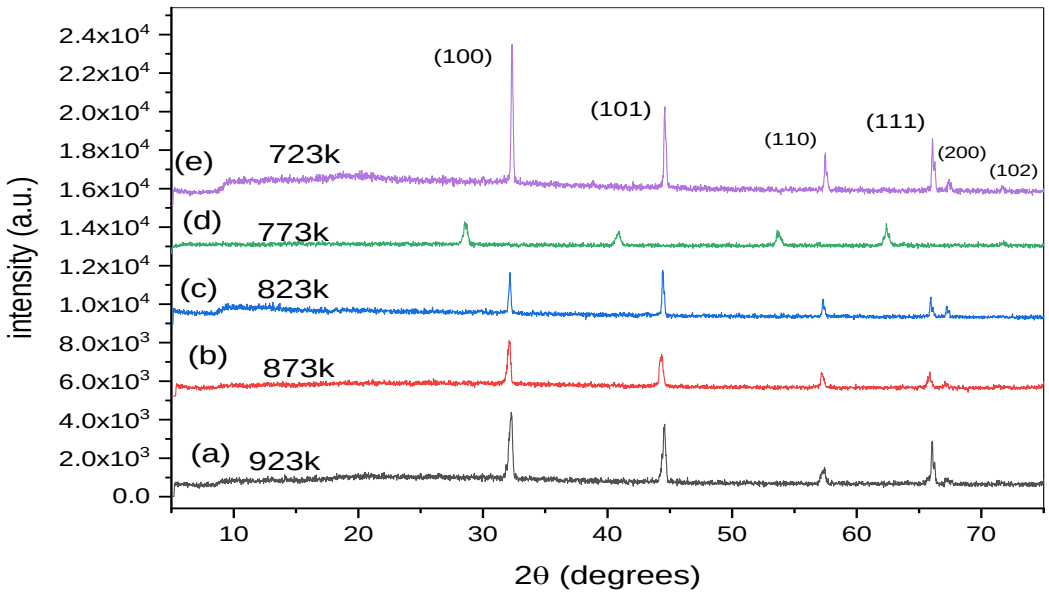

(Fig..1) : XRD patterns for all the sample Sn-2Ag-18In , **at (a) 923k , (b) 873k, (c) 823k ,(d) 773k and (e) 723k**

2Θ	d(A°)	I%	(hkl)
32.06	2.7894	100	(100)
44.32	2.0421	80	(101)
57.18	1.6096	15	(110)
65.84	1.4173	15	(111)
67.08	1.3941	10	(200)
71.41	1.3197	15	(102)

Table (1): X-ray diffraction patterns for 20%In-80%Sn Stander **(**JCPDS-ICDD) (PDF # 48-1547)

2Theta (º)	d (A)	I %	(hkl)	FWHM (º)	Grain size D (nm)	$D^2(nm)^2$	$\delta = 1/D^2 nm^{-2}$
32.12	2.7843	100	(100)	0.331	26.08496	680.42503	0.00147
44.5	2.0343	79.5	(101)	0.317	28.27967	799.74001	0.00125
57.38	1.6045	21.9	(110)	0.406	23.29644	542.72424	0.00184
66.22	1.4101	55.8	(111)	0.285	34.75645	1208.01101	8.27807E-4
67.38	1.3883	8.6	(200)	0.39	25.6314	656.96869	0.00152
71.881	1.3124	4	(102)	0.836	**Average= 27.609784**		

Table (2): The details of the XRD analysis particle size, dislocation density and lattice parameters.at temperature 923k.

2Theta (º)	d (A)	I %	(hkl)	FWHM (º)	Grain size D (nm)	$D^2(nm)^2$	$\delta = 1/D^2 nm^{-2}$
32	2.7946	100	(100)	0.33	26.15613	684.14326	0.00146
44.28	2.0439	80	(101)	0.31	28.89561	834.95603	0.0012
57.3	1.6066	35.8	110) (	0.315	30.01507	900.90419	0.00111
65.94	1.4154	30.8	111) (	0.351	28.17624	793.90035	0.00126
67.28	1.3905	10.9	200) (	0.303	32.89153	1081.85303	9.2434E-4
					Average= 29.226916		

Table (3): The details of the XRD analysis particle size, dislocation density and lattice parameters.at temperature 873k

2Theta (º)	d (A)	I %	(hkl)	FWHM (º)	Grain size D (nm)	$D^2(nm)^2$	$\delta = 1/D^2 nm^{-2}$
32.06	2.7895	77.5	(100)	0.258	33.46055	1119.60817	8.9317E-4
44.42	2.0378	100	(101)	0.262	34.20649	1170.08371	8.5464E-4
57.38	1.6045	38.2	(110)	0.261	36.23891	1313.25867	7.61465E-4
66.1	1.4124	45	(111)	0.256	38.66732	1495.16177	6.68824E-4
67.4	1.3883	25.6	(200)	0.279	35.74584	1277.76517	7.82616E-4
					Average= 35.663822		

Table (4): The details of the XRD analysis particle size, dislocation density and lattice parameters.at temperature 823k

2Theta (º)	d (A)	I %	(hkl)	FWHM (º)	Grain size D (nm)	$D^2(nm)^2$	$\delta = 1/D^2nm^{-2}$
28.44	3.1357	100	(100)	0.385	22.23225	494.27297	0.00202
40.76	2.2119	61.4	(101)	0.416	21.27694	452.70814	0.00221
53.7	1.7055	61.7	(110)	0.421	22.08964	487.95228	0.00205
62.42	1.4865	85.8	(111)	0.412	23.54652	554.43853	0.0018
71.82	1.3133	16.3	(102)	0.395	25.9346	672.60344	0.00149
					Average= 23.01599		

Table (5):The details of the XRD analysis particle size, dislocation density and lattice parameters.at temperature 773k)

Table (6):The details of the XRD analysis particle size, dislocation density and lattice parameters.at temperature 723k)

2Theta (º)	d (A)	I %	(hkl)	FWHM(º)	Grain size D (nm)	$D^2(nm)^2$	$\delta = 1/D^2nm^{-2}$
32.22	2.776	100	(100)	0.262	32.96295	1086.55634	9.20339E-4
44.56	2.0317	61.6	(101)	0.259	34.62	1198.5441	8.34346E-4
57.54	1.6004	28.1	(110)	0.262	36.12824	1305.24942	7.66137E-4
66.22	1.4101	42.4	(111)	0.26	38.09842	1451.48956	6.88947E-4
67.56	1.3854	9.1	(200)	0.365	27.34903	747.96929	0.00134
71.84	1.313	4	(102)	0.433	**Average= 33.831728**		

3.2. Particle size, dislocation density and lattice distortion :

The average particle size values were described in Table (7) The dislocation density calculated by using : -($\delta = \frac{1}{D^2}$ ... ... (2) (Williamson and Hall, 1953) . Its values were listed in table (7) The lattice distortions were studied and calculated according to(Williamson and Hall, 1953, Cullity, 1978). $\boldsymbol{\beta = \frac{1}{D} + 5 \leq \varepsilon^2 \geq \frac{1}{2} \sin \frac{\theta}{\lambda}}$**----(3)**, where: D is the crystallite size, and is local lattice distortion in the hexagonal matrix .

Temperatures:	Average (D)(nm)	$\delta = \frac{1}{D^2} nm^{-2}$
Sn-2Ag-18In at 923k	27.60978	0.00131
Sn-2Ag-18In at 873k	29.22692	0.00117
Sn-2Ag-18In at 823k	35.66382	7.8622E-4
Sn-2Ag-18In at 773k	23.01599	0.00189
Sn-2Ag-18In at 723k	33.83173	8.73678E-4

Table (7):The particle size, and dislocation density as function of prepared temperatures.

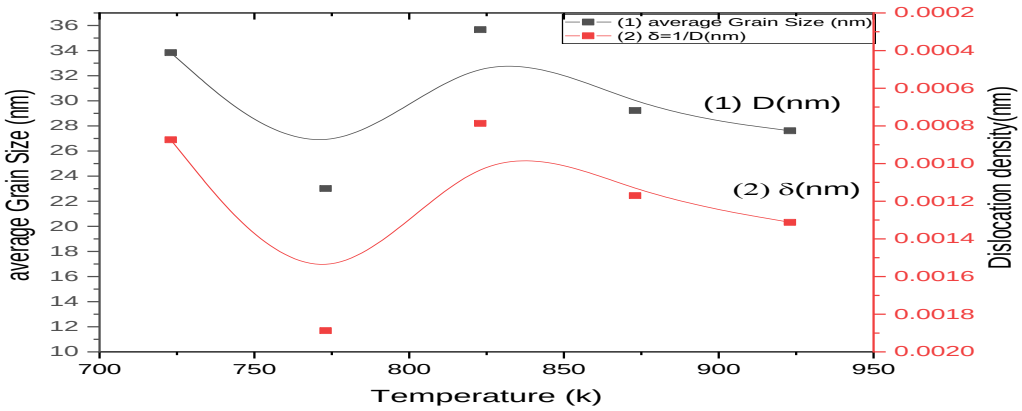

Fig (2): The particle size and dislocation density as function of prepared temperatures of the sample .

3.3.The X-ray density(D_x) and bulk density (D_b) :-

Sample no :	temperatures	D_x gm/cm^{-3}	D_b gm/cm^{-3}	a(nm)	c(nm)
Sn-2Ag-18In	923k	7.33	7.15	0.3215	0.2929
Sn-2Ag-18In	873k	7.23	7.23	0.3227	0.2996
Sn-2Ag-18In	823k	7.30	7.05	0.3221	0.2981
Sn-2Ag-18In	773k	6.61	6.6	0.3621	0.2604
Sn-2Ag-18In	723k	7.37	7.08	0.3205	0.2981

Table(8):The X-ray density(D_x) and bulk density (D_b) . As a function of preparation at room temperature .

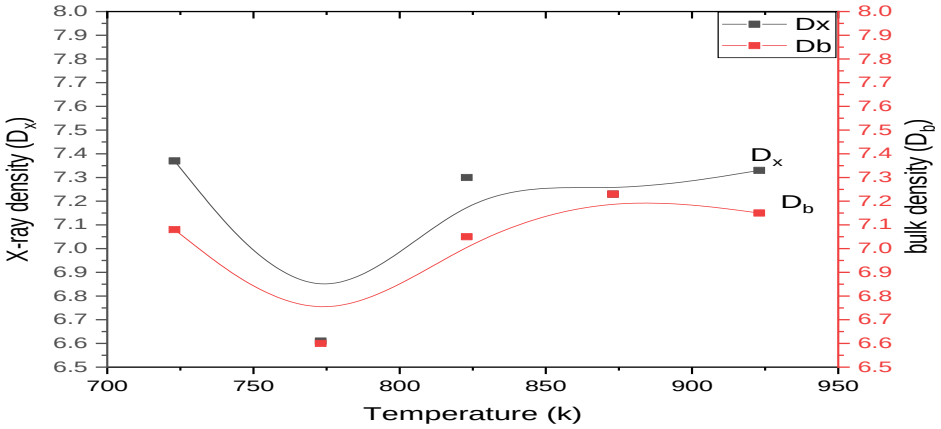

Fig (3): The X-ray density(D_x) and bulk density (D_b) as a function of preparation at temperature .

3.4. Mechanical Properties

3.4.1 Creep Strain- Tim

With regards to mechanical properties for the investigated materials, figures 4 (a , b & c) showed the creep strain-time curves for Sn-2Ag-18In alloys. The samples were investigated after.(T=923k,873k,823k ,773k , and 723k)and testing at temperatures of (T= 298k,323k and 353k) under three different constant stresses (= 6.2 , 8.7and 12.5 MPa). From figs 4 (a_1 and b_1), its presented that the creep time and resistance of Sn-2Ag-18In alloy with 6.2 MPa load and room temperature are the longest compared to other that of Sn-2Ag-18In alloys. Figs.4 (b_2), the creep time and resistance of Sn-2Ag-18In alloy with 8.7MPa load are the lowest compared to other that of the Sn-2Ag-18In alloys. In general, the creep resistance of Sn-2Ag-18In alloys was higher than of alloy, may be due to the refinement of structure and formation, and these mechanical improvements are attributed to the high structural stability of Sn-2Ag-18In alloys . The formations in the ternary alloys can result in impeding the dislocation movement more efficiently, and produce an alloy with lower creep rate. Similar phenomena that agree with Mahmudi et al, (Mahmudi et al., 2009) can be found for Sn-9Zn alloy with addition of Ag and AL . The creep strain rate of the Sn-2Ag-18In alloys was calculated by using the slope between Strain-Time Curves in the secondary stage as shown in Figures 4 .For three Alloys showed the three fold Stage of creep, while from Figs 4 the behavior of creep for Five Alloys were showed only in three creep stages. From Table(9) and Table(10)

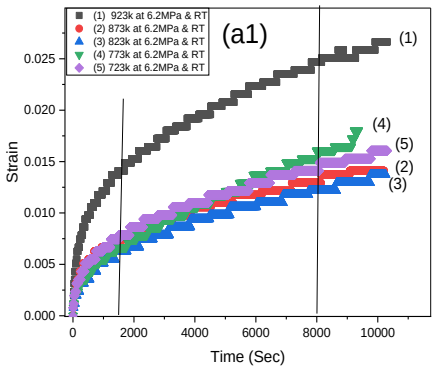
(1) 923k at 6.2MPa & RT
(2) 873k at 6.2MPa & RT
(3) 823k at 6.2MPa & RT
(4) 773k at 6.2MPa & RT
(5) 723k at 6.2MPa & RT
(a1)
Strain
Time (Sec)

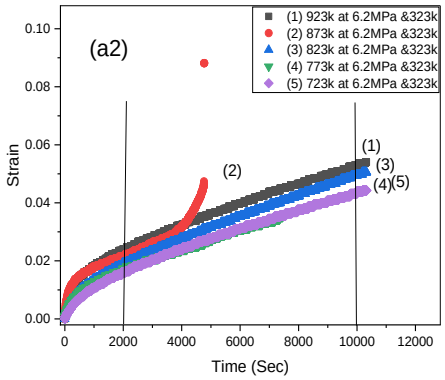
(1) 923k at 6.2MPa &323k
(2) 873k at 6.2MPa &323k
(3) 823k at 6.2MPa &323k
(4) 773k at 6.2MPa &323k
(5) 723k at 6.2MPa &323k
(a2)
Strain
Time (Sec)

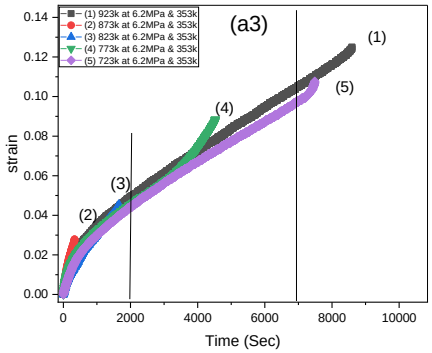
(1) 923k at 6.2MPa & 353k
(2) 873k at 6.2MPa & 353k
(3) 823k at 6.2MPa & 353k
(4) 773k at 6.2MPa & 353k
(5) 723k at 6.2MPa & 353k
(a3)
strain
Time (Sec)

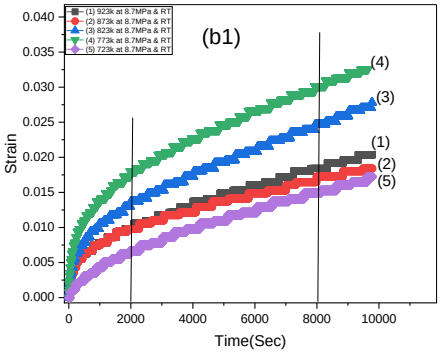
(1) 923k at 8.7MPa & RT
(2) 873k at 8.7MPa & RT
(3) 823k at 8.7MPa & RT
(4) 773k at 8.7MPa & RT
(5) 723k at 8.7MPa & RT
(b1)
Strain
Time(Sec)

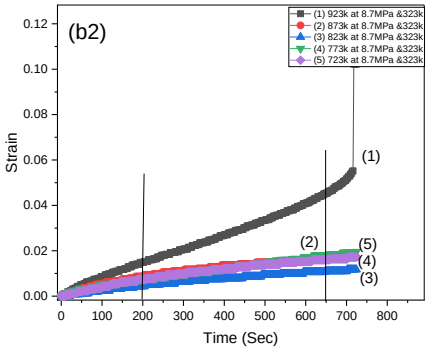
(1) 923k at 8.7MPa &323k
(2) 873k at 8.7MPa &323k
(3) 823k at 8.7MPa &323k
(4) 773k at 8.7MPa &323k
(5) 723k at 8.7MPa &323k
(b2)
Strain
Time (Sec)

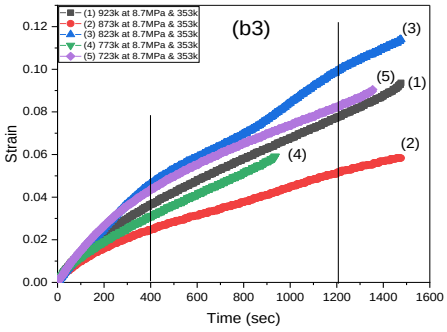
(1) 923k at 8.7MPa & 353k
(2) 873k at 8.7MPa & 353k
(3) 823k at 8.7MPa & 353k
(4) 773k at 8.7MPa & 353k
(5) 723k at 8.7MPa & 353k
(b3)
Strain
Time (sec)

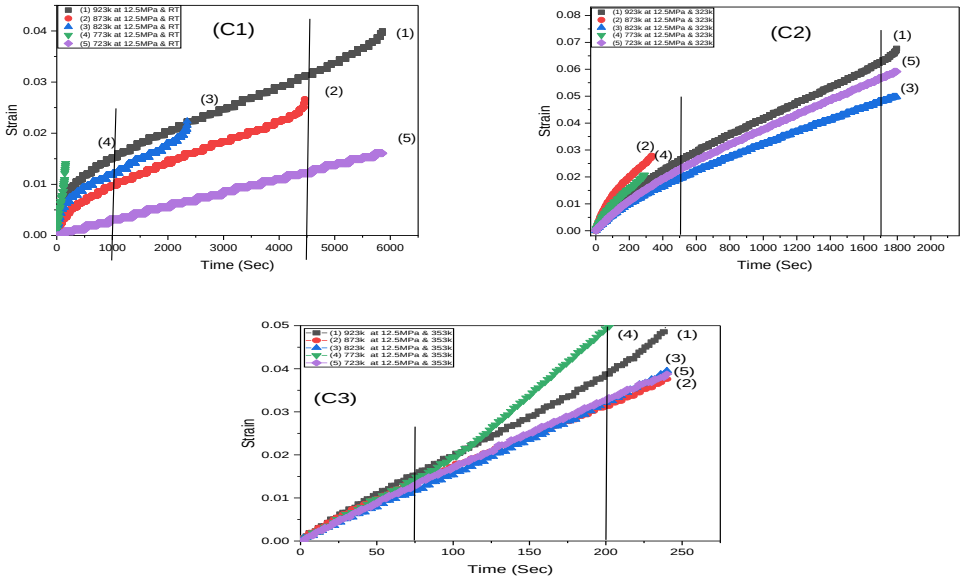

Figs. (4) Creep strain-time curves for Sn-2Ag-18In at **a**) (a1 , a2 , a3), **b**) (b1, b2, b3) **C**)(C1, C2, C3) , at (298k,323k and 353k) , at(6.2 , 8.7 and 12.5MPa)

Samples in Wt.%	**Creep rate(S-1) at 6.2 MPa**			**Creep rate(S-1) at 8.7 MPa**			**Creep rate(S-1) at 12.5 MPa**		
Tem.	**298k**	**323k**	**353k**	**298k**	**323k**	**353k**	**298k**	**323k**	**353k**
Sn-2Ag-18In at 923k	**1.51428E-6**	**3.68236E-6**	**1.10395E-5**	**1.39908E-6**	**6.42265E-5**	**5.0066E-5**	**4.35207E-6**	**2.97674E-5**	**1.82397E-4**
Sn-2Ag-18In at 873k	**7.90551E-7**	**4.32112E-6**	**1.10395E-5**	**1.13685E-6**	**8.42905E-6**	**3.07712E-5**	**4.21547E-6**	**3.21357E-5**	**1.42265E-4**
Sn-2Ag-18In at 823k	**8.59275E-7**	**3.89082E-6**	**2.12905E-5**	**1.82922E-6**	**8.06241E-6**	**6.02183E-5**	**5.57578E-6**	**2.45012E-5**	**1.74156E-4**
Sn-2Ag-18In at 773k	**1.33764E-6**	**3.39682E-6**	**1.2167E-5**	**1.99933E-6**	**8.46086E-6**	**5.30073E-5**	**5.54106E-5**	**5.51278E-5**	**3.04225E-4**
Sn-2Ag-18In at 723k	**9.22718E-7**	**3.36534E-6**	**1.04889E-5**	**1.34602E-6**	**7.90594E-6**	**4.8368E-5**	**2.73807E-6**	**2.92909E-5**	**1.49455E-4**

Table (9): The variation of creep rate of five samples(Sn-2Ag-18In) with Temperature (923k,873k,823k,773k , and 723k) .

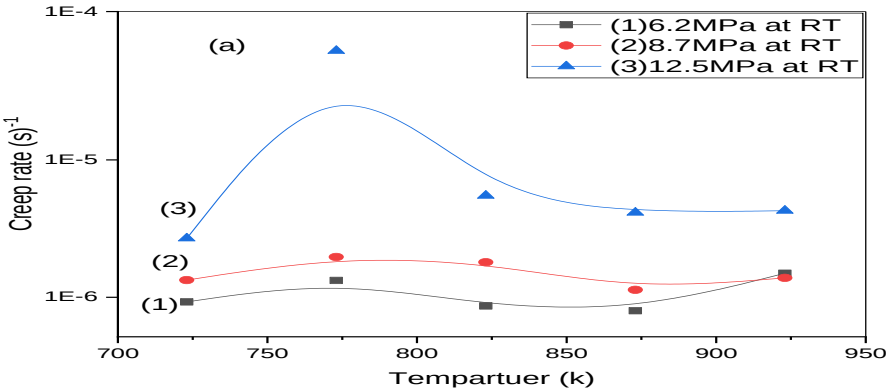

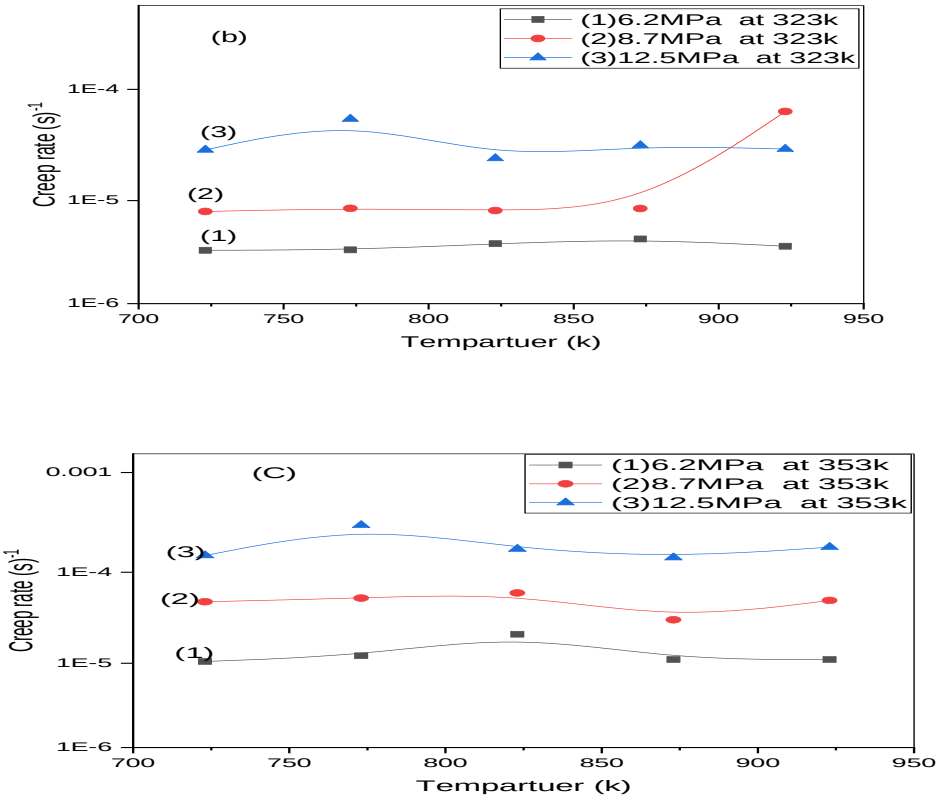

Fig. (5) The creep rate (S^{-1}) ,(a) , (b), (C) for Sn-2Ag-18In at T= 298k, 323kand 353k under 6.2 , 8.7 and 12.5 Mpa

Table (10): The variation of elongation of three samples with Temperatures addition

Sample no:	EL(%)								
Temperature	6.2MPa			8.7 MPa			12.5MPa		
Tem .	298k	323k	353k	298k	323k	353k	298k	323k	353k
Sn-2Ag-18In at 923k	0.60168	0.84893	1.79099	0.33297	1.2576	1.55606	0.00825	0.23153	0.19895
Sn-2Ag-18In at 873k	0.4321	0.83627	1.44635	1.20112	1.22168	0.67195	0.10783	0.2503	-0.67692
Sn-2Ag-18In at 823k	0.45765	1.00918	0.54466	0.84276	0.69317	1.12462	0.54469	-0.06082	-0.13713
Sn-2Ag-18In at 773k	0.59456	1.48237	2.25052	0.66248	0.87462	1.02144	0.4571	0.83491	0.19943
Sn-2Ag-18In at 723k	1.12106	1.48237	2.25052	0.64621	0.0264-	1.16244	0.94444	0.77651	0.07494

The Elongation (El.%) was calculated for all the figures 6(a to c), by using equation: **(EL.%= Strain × 100) --- (4)**. The El.% plots are drawn in Fig (6), and its values were listed in the Table (10) for three alloys The Elongation of Sn-2Ag-18In alloy at T=289, 323and 353k with 6.2, 8.7 and12.5MP as shown in Fig.(6). The EL.%(a), (b)of Sn-2Ag-18In at T=298k, 323k and 353k under 6.2 , 8.7 and 12.5 MPa are increasing compared to The EL.% of Sn-2Ag-18In at the same load as shown in fig.(6) (a ,b, c).

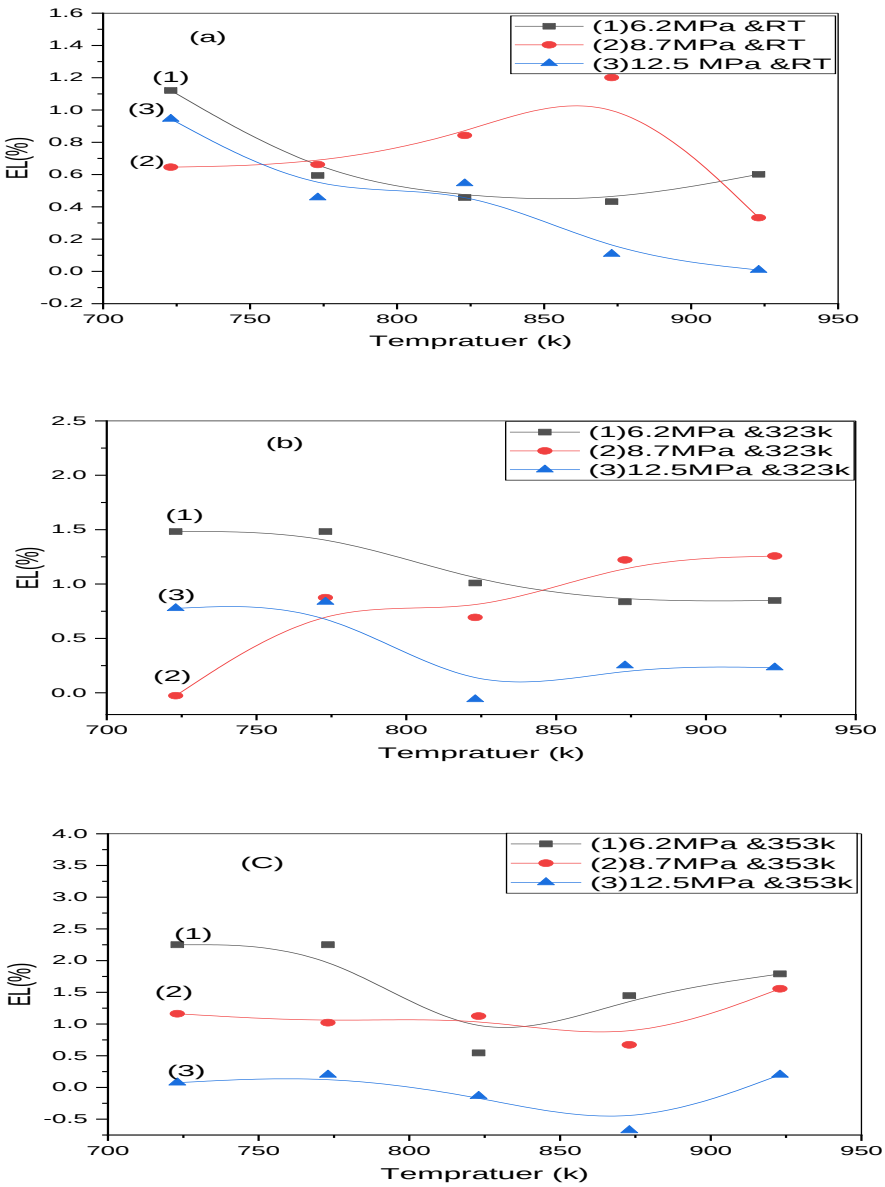

Fig. (6). The El. (%) , (a) , (b) and (c) for Sn-2Ag-18In at (T= 298k ,323k and 353k) under 6.2 , 8.7 and 12.5 MPa

3.4.2. Creep stress exponents and activation energy for Sn-2Ag-18In Alloys:-

The stress exponent (n) parameter and activation energy(Q) of steady state creep were calculated by using equations: (Rahman et al., 2009): $\mathbf{(n = \frac{\partial \ln(\dot{\varepsilon})}{\partial \ln(\sigma)})}$ **-- (5)**and $\mathbf{Q=-R(\frac{\partial \ln(\dot{\varepsilon})}{\partial \ln(\frac{1}{T})})}$**-(6)** . The calculated values of n and Q at different temperatures and loads for the tested alloys are listed in the table (11 and 12) and, compared to the Alloy literature review. The differences between n and Q values may vary in the preparation method and the heat treatment method. The results of the

values of stress exponents, as shown in Fig.(7)and given in table (11) that compared with literature review for alloy, at different temperatures (923k, 873k,823k,773k , and 723k) its decrease from n=(2.2 , 2.316 , 5.66 and 2.9) at T= 289k , n= (3.003 , 2.583, 2.695 , and 3.09) at T= 323k and n= (3.991 , 3.633 , 2.812 , and 3.52) at T=353k for Sn-2Ag-18In respectively. The difference between n values for all alloys at different temperatures is due to the dislocation movement (climb- creep) mechanism ,as documented by (Kanda and Kariya ,. 2012 and Wiese et al., 2008) While, at temperature (T=353k) the n value of Sn-2Ag-18In alloy is due to the dislocation movement (slip-creep) mechanism. Also, the activation energies in steady state creep of three alloys were calculated from the slope of relation between Ln (Creep rate) and 1000/T at(T=289k ,323k and353k) in the Figs. 9 (a, b and c), with two different applied stresses. It is noticeable that Q decreases with the increase of applied stress that depends strongly on applied stress and temperatures(Wu and Huang, 2002). The Q increases with increasing In addition to Sn-2Ag alloy. It was observed that Sn-2Ag-18In has the highest Q values depending on creep resistance, as documented by (Mahmudi et al., 2009, Khalifa et al., 2017 and El-Daly , Hammad, 2010).

Sample no:	n			m		
temperatures	RT	323k	353k	RT	323k	353k
S2Ag-18In at 923k	**1.58103**	**3.03116**	**2.19283**	**0.6325**	**0.32991**	**0.45603**
S2Ag-18In at 873k	**2.42065**	**2.89724**	**2.22075**	**0.41311**	**0.34516**	**0.4503**
S2Ag-18In at 823k	**2.69778**	**2.65479**	**1.48787**	**0.37068**	**0.37668**	**0.6721**
S2Ag-18In at 773k	**0.57514**	**1.30598**	**2.10606**	**1.73871**	**0.76571**	**0.47482**
S2Ag-18In at 723k	**3.50052**	**3.12178**	**3.82269**	**0.28567**	**0.32033**	**0.2616**

Table (11)and stress exponent (n) values for Sn–2Ag-18In solder alloys at temperatures (923k,873k,823k,773k , and 723k) . And (m values for Sn-2Ag-18In .

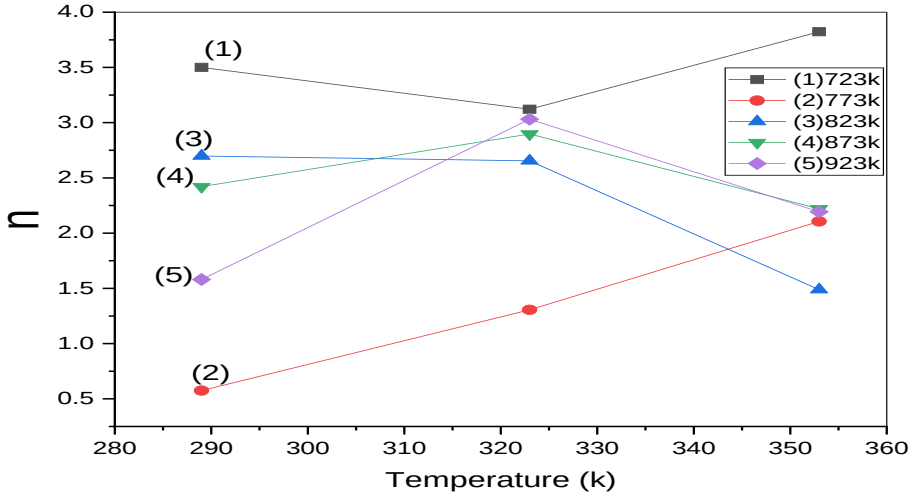

Fig. (7): The stress exponent(n) values at different temperature with Sn-2Ag-18In , at temperatures (923k,873k,823k,773k , and 723k).

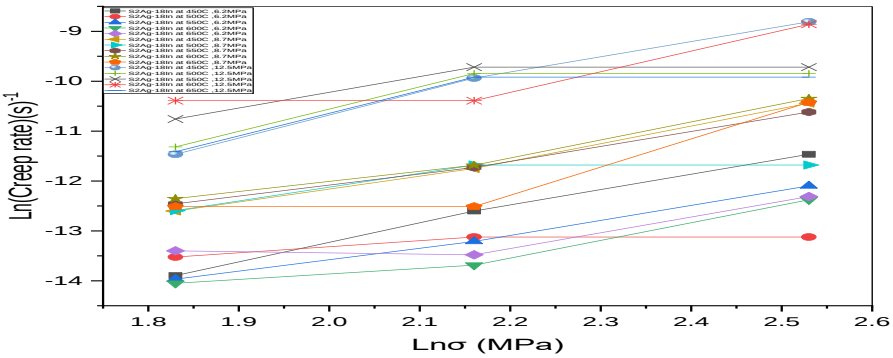

Fig(8):Relay between Ln(Creep rate) versus Ln(Stress) at different temperatures (298 – 323 – 353) K for (Sn- 2Ag – 18In) .

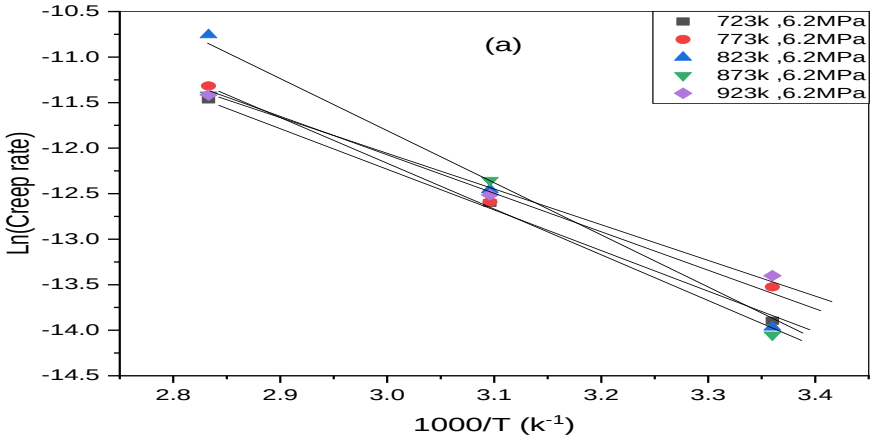

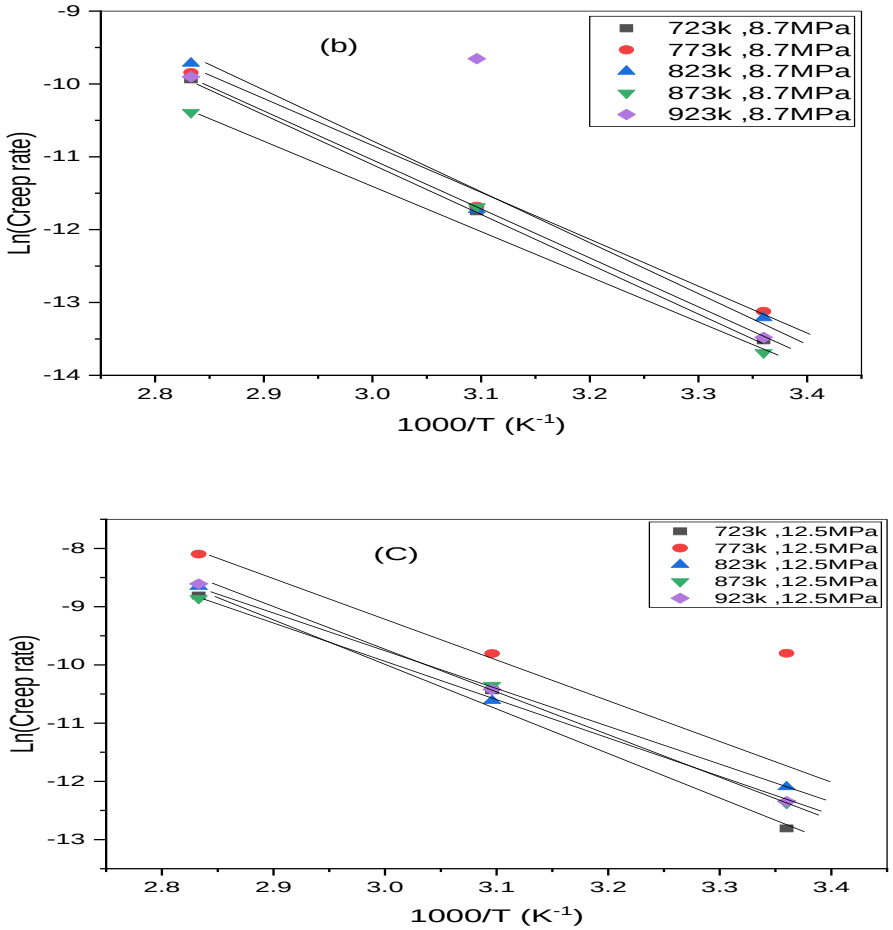

Fig. (9) The relation between Ln($\dot{\varepsilon}$) and 1000/T for Sn-2Ag-18In Alloys at(a)6.2 MPa and(b) 8.7 MPa and (c) 12.5 MPa.

Sample no :	Q (ev)		
	6.2MPa	8.7MPa	12.5MPa
S2Ag-18In at 923k	**0.7778**	**1.49278**	**1.07062**
S2Ag-18In at 873k	**1.19591**	**1.43381**	**1.09367**
S2Ag-18In at 823k	**1.33649**	**1.31504**	**0.74361**
S2Ag-18In at 773k	**0.28744**	**0.6527**	**1.05256**
S2Ag-18In at 723k	**1.73745**	**1.54633**	**1.89904**
Average	**1.06702**	**1.28813**	**1.1719**

Table(12): Activation energy (Q)

Isothermal creep test for Sn-2Ag-18In solder alloys was carried out at three constant applied stresses (6.2 , 8.7 , and 12.5 MPa) and three test temperature (298 , 323 and 353K). The creep behavior observed at low temperature has three choral touristic stages .A region of initial (of elastic unsteady) creep , in which the rat of creep varies rapidly , the second region in which the rat of creep remains constant (steady state) creep and finally a third region in which the rat of creep varies rapidly (rupture region) which is followed by failure as shown in fig(9) The steady state creep rate $\acute{\varepsilon}_s$ calculated from the slopes of the linear regions of the creep curves ,increases with increasing applies stresses and test temperature the variation in strain rates (creep rates) is the result of changes in the internal structure of the material with creep strains and time . The relationship of y stress –strain of samples is visually expressed by the following equation with in the steady state region .$\acute{\varepsilon}_s = A\ \sigma^n$ where **A** is a constant and **n** is stress exponent . A plot of logarithm of $\acute{\varepsilon}_s$ versus the logarithm σ yields a straight curve with slope (n)which determines the mechanism of creep defamation A commonly equation by design engineers for stress and temperature dependence of creep (strain)rate especially in the electronics industry is the Norton power law (D.mitlin et al)

$\varepsilon'_s = A\sigma^n\ e^{\frac{-Q}{RT}}$ Where ε'_s is the steady state strain rat A is a constant ,σ is the stress , n is the stress exponent , Q is the activation energy .**R** is the universal gas constant , and **T** is the absolute temperature. The stress exponent (n) determines the type of defamation mechanism (viscous glide , screw dislocation , climb mechanism , etc .) . The transition form viscous glide to dislocation climb (n≈1 to n ≥ 3) .The values of $\acute{\varepsilon}_s$ increased with increasing the applied stress and the test temperature for all alloys . The increase of $\acute{\varepsilon}_s$ with increasing with increasing test temperature could be explained in view of an easier motion of dislocations already existing ,where the thermal energy introduced facilitates the dislocation motion by helping it to overcome the precipitates which act as barriers . The values of the stress exponent n for Sn-2Ag-18In between 0.5 and 3.8 .The activation energy of the stead creep of the alloys which were calculated .It is found that the value of the activation energy in the range (0.287-1.899 ev), which is depending on the prepared temperature of alloys and particularly in the case of rode-like microstructure . According to the data presented in the mechanical behavior of the solder alloys is affected by intermetallic precipitation .It is clear that due to the presence of intermetallic precipitation the activation energy for alloys creep shoulder be higher and lower .

3.4.3. Electrical resistivity and conductivity

With respect to electrical properties, electrical resistivity(**ρ**) an conductivity (**σ**)were calculated by using equations: $\boldsymbol{\rho = R\frac{A}{L}}$ **-- (7) and** $\boldsymbol{\sigma = \frac{1}{\rho}}$ **--- (8),** receptively, Where L is length of the specimen ,R is the ohm resistance and A is the cross-section area(Callister, 2007, La Barre, 2004). The electrical resistivity and conductivity of Sn-2Ag-18In alloys at room temperature (T=298k) are shown in table (12) and fig. 10(a& b), in general the ρ values have decreased with In additions, but the σ values have increased with In additions. This decrease and increase for ρ and σ are may be due to enhancing the In0.2Sn0.8 and Ag4Sn formation in Sn-2Ag Alloys with 18In-Additions. The eutectic temperature reaches about 473k when the In content 16Wt % Sn-3.5Ag-16In . (S.E.Negm et al) . It can be suggested that the eutectic temperature of the samples prepared reaches about 470k when the In content 18Wt% which is the working melting point of the common soldering alloy .

Sample no :	temperatures	**ρ (Ω .Cm) * 10^3**	**Ϭ $(Ω . Cm)^{-1}$ *10^{-4}**
S2Ag-18In	923k	1.135	8.81
S2Ag-18In	873k	1.241	8.06
S2Ag-18In	823k	1.147	8.718
S2Ag-18In	773k	1.156	8.65
S2Ag-18In	723k	1.130	8.849

Table (13): The variation of (ρ) and (σ) for five samples with temperatures, at room temperature (T= 298k).

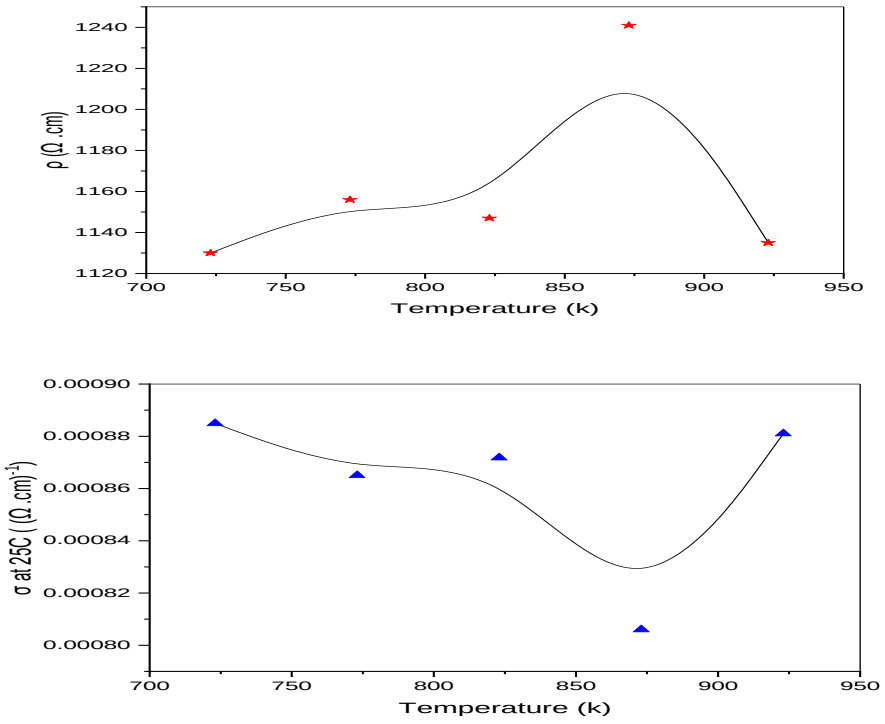

Fig. (10): (a) Electrical resistivity behavior for Sn-2Ag-18In alloys with temperatures at T= 298k and, (b) Electrical conductivity behavior for Sn-2Ag-18In alloy with temperatures additions at T= 298k

4. Conclusions

This study has investigated the Indium(In) improvements in two concentrations (18wt.%) the alloy solders (Sn-Ag-In) at different temperatures(923k,873k,823k,773k,and 723k) to investigate some of their structure and different Mechanical properties as function of load and temperature ,The X-ray diffraction analysis of the samples ensures the formation of single phase tetragonal ,The average particle size estimated is(23.016 – 35.664)nm. Values of stress exponents (n) were found to be in the range of 0.575 to3.822 for all alloys. Values of activation energy (Q) of alloys were found to be in the range of 0.287 to 1.737 ev for σ =6.2MPa and 0.652 to 1.546 ev for σ =8.7MPa and 0.743 to 1.899 ev for σ =12.5MPa , The electrical conductivity of samples was calculated at room temperature (298k), its values increased with In-additions .on the structural, Mechanical (Creep resistance) and electrical conductivity properties of Sn-2Ag-18In alloy. The results are summarized as follows. With the addition of 18In to Sn-2Ag alloys leads to the formation of hexagonal. The average particle size (D) of In0.2Sn0.8 phases decreased continuously with addition of (18% In), while The dislocation density (δ) increased with In-additions. The creep resistance of Sn-2Ag-18In Alloys are higher than that of at different temperature (923k,873k, 823k, 773k , and 723k) loads due to the refinement structure and formation of new single phase . The n values are due to that the deformation mechanism and the dislocation climb for all alloys at different temperatures, except at T= 773k prepared temperature for Sn-2Ag-18In alloy, the dislocation movement (slip-creep) is controlling mechanism. In general, increasing of Q with (18In)-addition to Sn-2Ag Alloys depends on creep resistance. Also, the decrease of Q with the increase of applied stress depends strongly on applied stress and temperature. The decrease and increase for ρ and are may be due to enhancing precipitation formation in Sn-2Ag Alloys with In-additions .And the joint reliability of the Sn-2Ag-18In solder is comparable to that of Sn-Pb eutectic solder, thereby making this solder a potential candidate for extension of the lead-free circuit manufacturing process, (Guod et al., 2014).

Reference

[1]. AHMED, M., FOUZDER, T., SHARIF, A., GAIN, A. K. & CHAN, Y. C. (2010). Influence of Ag micro-particle additions on the microstructure, hardness and tensile properties of Sn–9Zn binary eutectic solder alloy. *Microelectronics Reliability*, 50**,** 1134-1141.

[2] CALLISTER, W. D. (2007). *Materials science and engineering an introduction*, John Wiley.

[3]. CHEN, W., XUE, S., WANG, H., WANG, J. & HAN, Z. (2009). Solderability and intermetallic compounds formation of Sn-9Zn-xAg lead-free solders wetted on Cu substrate. *Rare Metals* .656,28 ،90 . and WILLIAMSON, G. & HALL, W. (1953). X-ray line broadening from filed aluminium and wolfram. *Acta metallurgica*, 1**,** 22-31.

[4]. CHENG, S., HUANG, C.-M. & PECHT, M. (2017). A review of lead-free solders for electronics applications. *Microelectronics Reliability*, 75**,** 77-95.

[5]. CULLITY, B. (1978). Elements of X-ray Diffraction. Addison and Wesley Publishing Company Inc. *Reading, USA***,** 32-106

[6]. EL-DALY, A., DESOKY, W., SAAD, A., MANSOR, N., LOTFY, E., ABD-ELMONIEM, H. & HASHEM, H. (2015). The effect of undercooling on the microstructure and tensile properties of hypoeutectic Sn–6.5 Zn–xCu Pb-free solders. *Materials & Design*, 80**,** 152-162
[7]. EL-DALY, A. & HAMMAD, A. (2010). Effects of small addition of Ag and/or Cu on the microstructure and properties of Sn–9Zn lead-free solders. *Materials Science and Engineering*: A, 527**,** 5212-5219.
[8]. EL-DALY, A., HAMMAD, A., AL-GANAINY, G. & IBRAHIEM, A. (2014). Design of lead-free candidate alloys for low-temperature soldering applications based on the hypoeutectic Sn–6.5 Zn alloy. *Materials & Design* (1980-2015), 56**,** 594-603. [9]. GAIN, A. K. & ZHANG, L. (2016). Harsh service environment effects on the microstructure and mechanical properties of Sn–Ag–Cu-1 wt% nano-Al solder alloy.
Journal of Materials Science: *Materials in Electronics*, 27**,** 11273-11283.
[10]. GAIN, A. K. & ZHANG, L. (2020). Nanoindentation Creep, Elastic Properties, and Shear Strength Correlated with the Structure of Sn-9Zn-0.5 nano-Ag Alloy for Advanced Green Electronics. *Metals*, 10**,** 1137
[11] (Materials Transactions, Vol. 45, No. *The Japan Institute of Metals*) #20044 (2004) pp. 1282 to 1289
[12] Williamson , G. K., and W. H. Hall, (1953) "X-ray line broadening from filed aluminium and wolfram," *Acta Metall.*, vol. 1, no. 1, pp. 22–31, [13]. GUODA, E., MAHASI, A., HADADI, K. & FAQEEH, A. (2014). Study the structure and electrical properties of Sn-9Zn-1Ag solder alloy. *International Journal of Physics and Astronomy*, 2**,** 123-128.
[14]. HAMADA, N., HAMADA, M., UESUGI, T., TAKIGAWA ،Y. & HIGASHI, K. (2010). Effect of small addition of zinc on creep behavior of tin. *Materials transactions***,** 1009131184-1009131184.
[15]. HAMMAM, M., ALLAH, F. S., GOUDA, E. S., EL GENDY, Y. & AZIZ, H. A. (2010). Structure and properties of Sn-9Zn Lead-free solder alloy with heat treatment. *Engineering*, 2**,** 172-178.
[16]. ISMAIL, R. A. (2020). Investigation of Microstructure and Mechanical Properties of Different Nano-Particles Doped Sn-Zn Lead-Free Solder Alloys. *Arab Journal of Nuclear Sciences and Applications*, 53**,** 191- .799
[17]. KANDA, Y. & KARIYA, Y. (2012). Evaluation of creep properties for Sn–Ag–Cu micro solder joint by multi-temperature stress relaxation test. *Microelectronics Reliability*, 52**,** 1435-1440.
[18]. KHALIFA, B., ISMAIL, R. A. & YASSIN, A. (2017). Structure Analysis, Enhancement of Creep Resistance and Thermal Properties of Eutectic Sn-Ag Lead-Free Solder Alloy by Ti and Cd Additions. *Journal of Advances Physics*, 1**,** 5092-5099.
[19]. KNOTT, S. & MIKULA, A. (2002). Thermodynamic properties of liquid Al-Sn-Zn alloys: A possible new lead-free solder material. *Materials transactions*, 43**,** 1868-1872.
[20]. KOTADIA, H. R., HOWES, P. D. & MANNAN, S. H. (2014). A review: On the development of low melting temperature Pb-free solders. *Microelectronics Reliability*, 54**,** 1253-1273.
[21] LA BARRE, K. A. (2004) .The Art and Science of Classification: Phyllis Allen Richmond, 1921—1997.
[22]. LIU, C.-Y., HON, M.-H., WANG, M.-C., CHEN, Y.-R., CHANG, K.-M. & LI, W.-L. (2014). Effects of aging time on the mechanical properties of Sn–9Zn–1.5 Ag–xBi lead-free solder alloys. *Journal of alloys and compounds*, 582**,** 229-235.
[23]. MAHMUDI, R., GERANMAYEH, A., NOORI, H. & TAGHADDOSI, M. (2009). Effects of Ag and Al additions on the structure and creep properties of Sn-9Zn solder alloy. *Journal of electronic materials*, 38**,** 330-337.
[24]. PENG, F., LIU, W., MA, Y., LIANG, C., HUANG, Y. & TANG, S. (2019). Microstructure of Sn-20In-2.8 Ag solder and mechanical properties of joint with Cu. *Soldering & Surface Mount Technology*.
[25]. RAHMAN, M., SHARIF, A. & AHMED, M. (2009). Effect of various

amount of Cu on the thermal and mechanical behavior of Sn-9Zn eutectic Pb-free solder alloy. *Proceedings of the International Conference on Mechanical Engineering* (ICME2009),. 26-28.

[26]. SALEM, D. (2020). Influence of Cu Addition on the Transient Creep Characteristics of Sn–9Zn-1.5Ag Solder Alloy. *American Research Journal of Physics*, 6**,** 1-11.

[27]. SHRESTHA, T., GOLLAPUDI, S., CHARIT, I. & MURTY, K. L. (2014). Creep deformation behavior of Sn–Zn solder alloys. *Journal of Materials Science*, 49**,** 2127-2135.

[28]. VUONG, B., VU, N., MANH ،T., VAKA, M., DU, D. & NAM, N. (2018). Role of cerium in microstructure and corrosion properties of Sn-1.0 Ag solder alloys. *Materials Letters*, 228**,** 309-313.

[29]. WIESE, S., ROELLIG, M., MUELLER, M. & WOLTER, K.-J. (2008). The effect of downscaling the dimensions of solder interconnects on their their creep properties. *Microelectronics Reliability*, 48**,** 843-850.

[35] S. Farina, C. Morando, Comparative corrosion behavior of different Sn-based solder
alloys, *J. Mater. Sci. Mater. Electron*. 26 (2014) 464–471.

[36] D.R. Flanders, E.G. Jacobs, R.F. Pinizzotto, *J. Electron. Mater*. 26 (1997) 883.

[39] Shakib .Alsowidy, Ahmed M. Aljarbani , Mohammed S. Gumaan ,Microstructural and Creep Characterization of Sn-0.7Cu and Sn-0.7Cu-xBi Lead-free Solders for Low Cost Electronic Applications, *Research Article*, February 23rd, 2021.

[40]. ZHU, W.,ZHANG, W., ZHOU, W. & WU, P. (2019). Improved microstructure and mechanical properties for SnBi solder alloy by addition of Cr powders. *Journal of Alloys and Compounds*, 789**,** 805-813.

[30]. WILLIAMSON, G. & HALL, W. (1953). X-ray line broadening from filed aluminium and wolfram. *Acta metallurgica*, 1**,** 22-31

[31]. WU, C. L. & HUANG, M. (2002). Creep behavior of eutectic Sn-Cu lead-free solder alloy. *Journal of electronic materials*, 31**,** 442-448.

[32]. XU, K.-K., ZHANG, L., GAO, L.-L., JIANG, N., ZHANG, L. & ZHONG, S.-J. (2020). Review of microstructure and properties of low temperature lead-free solder in electronic packaging. *Science and Technology of Advanced Materials*, 21**,** 689-711. [33]. ZHANG, L. & TU, K.-N. (2014). Structure and properties of lead-free solders bearing micro and nano particles. *Materials Science and Engineering: R: Reports*, 82**,** 1-32.

[34]. ZHAO, M., ZHANG, L., LIU, Z.-Q., XIONG, M.-Y. & SUN, L. (2019). Structure and properties of Sn-Cu lead-free solders in electronics packaging. *Science and technology of advanced materials*,20**,**421-444.

[37] Report Lead-Free Solders NASA Part and Packaging Program Goddard Space Flight Center Greenbelt, Maryland 1996.

[38] D.mitlin , C.H.Reader ,R.W.Messler ,*Metali* .Trans . A30 (1999) 115

[41] A. Milosavlevic, D. zivkovic, Z. Kamberovic, Metalurgija—*J. Metall.* 14 (3) (2008) 161–167.

[42] M.M. EL-Bahay, M.E.L. Mossalamy, M. Mahdy, A.A. Bahgat,
J. Mater. Sci.: Mater.Electron. 15 (2004) 519–526.

[43] D.mitlin , C.H.Reader ,R.W.Messler ,*Metali* .Trans . A30 (1999)115.

[44] S.E.Negmetal / *Journal of Alloys and compounds* 503(2010) 65-7